Elektronisches Rauschen

Versuch zum Fortgeschrittenen-Praktikum

Physikalisches Institut

Johann Wolfgang Goethe-Universität

Frankfurt am Main

Version Oktober 2018

Betreuer-Kontaktdaten

Merlin Mitschek

Raum-Nr.:	_ _.328
Tel.:	47288
E-Mail:	mitschek@physik.uni-frankfurt.de
Arbeitsgruppe:	Prof. J. Müller

Ort des Versuchs: Laborraum der AG Müller, _ 0.426

Worum geht's?

Elektronisches Rauschen von ohmschen Widerständen und eines quasi-2D molekularen Metalls (organisches Ladungstransfersalz)

Wie wird's gemacht?

Messung der Spannungsfluktuationen dieser verschiedenen Systeme mittels eines Signalanalysators:

- unterschiedliche ohmsche Widerstände (evtl. bei verschiedenen Temperaturen)
- molekulares Metall (organisches Ladungstransfersalz)

Was wird gelernt?

Verschiedene Arten elektronischen Rauschens, Signal-Rausch-Verhältnis, Zeitreihenanalyse (spektrale Leistungsdichte des Rauschens mittels Fourier-Transformation) und Korrelationsfunktionen

Wofür ist das interessant?

Messtechnik: Verbesserung der Empfindlichkeit, Auflösung, Genauigkeit physikalischer Messungen; Fluktuationsspektroskopie

Physik: Verständnis der Ursachen von elektronischen Fluktuationen, Verständnis der Dynamik von Störstellen in Halbleitern und der intrinsischen Ladungsträgerdynamik in korrelierten Elektronensystemen;

Allgemeines: Erfahrung im Umgang mit Fluktuationen, stochastischen Prozessen und Zeitreihen → Anwendungen z.B. in der Statistik und in der Finanzmathematik

Elektronisches Rauschen

I. Allgemeine Bemerkungen

Die meisten Menschen (sogar die meisten Physiker) werden im Phänomen des Rauschens etwas Negatives, zumindest jedoch etwas Lästiges sehen, denn z.B. in elektrischen Messungen wird die ultimative Messgenauigkeit limitiert durch Rauschen, Schwankungserscheinungen, Fluktuationen: ein zu messendes Spannungssignal muss mindestens größer sein als die mittlere Schwankung des Signals mit der Zeit, damit es noch zuverlässig aufgelöst werden kann. Physiker sind deshalb in den allermeisten Fällen daran interessiert, das Rauschen/die Fluktuationen soweit als möglich zu unterdrücken. Um das auf systematische Weise bewerkstelligen zu können, müssen die physikalischen Ursachen des Rauschens allerdings zunächst verstanden werden!
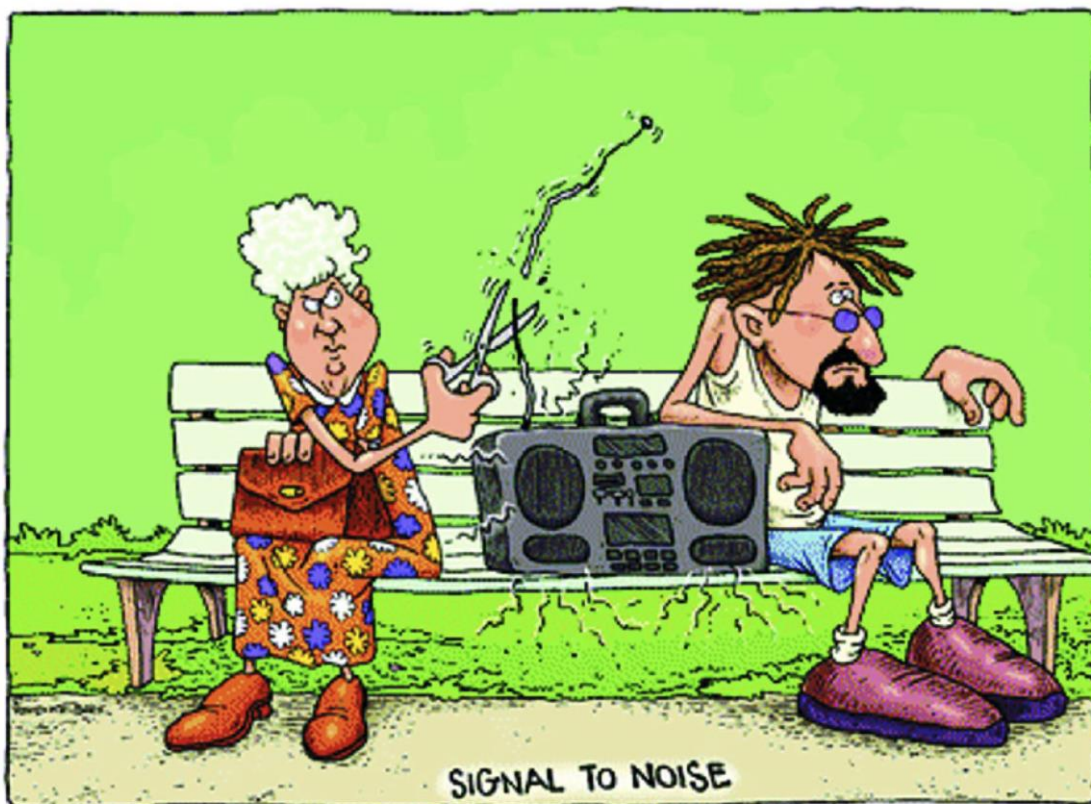
„Whether noise is a nuisance or a signal may depend on who you ask. [...]"
aus: Beenakker, Schönenberger, *Physics Today* (May 2003)

Ein zweiter Grund, warum es sich lohnt, die Fluktuationen einer physikalischen Größe und insbesondere das elektronische Rauschen in Festkörpern zu untersuchen: Im Rauschen sind wertvolle Informationen über die intrinsischen, dynamischen Eigenschaften der Ladungsträger enthalten, die man allerdings zunächst einmal sichtbar machen muss. (Glücklicherweise gelingt dies bereits durch eine einfache Fourier-Transformation.) Betracht man das *Rauschen als* das eigentliche *Signal*, zieht also aus dem vermeintlichen Ärgernis (siehe obigen Cartoon) einen Nutzen, so ergeben sich neue Perspektiven!

Fluktuationen treten grundsätzlich und fundamental in allen physikalischen Größen auf und sind naturgemäß *zufällig* (statistisch); **die spektrale Leistungsdichte S** der Fluktuationen allerdings ist eine *statistisch stationäre* (nicht-zufällige) Größe, die wiederum mit der sog. Autokorrelationsfunktion der fluktuierenden physikalischen Größe verknüpft ist (über eine Fourier Transformation). Messen wir also die spektrale Leistungsdichte der Spannungs-Fluktuationen einer Probe, so erhalten wir indirekt Zugriff auf die Spannungs-Autokorrelationsfunktion, worin Information über die dynamischen Eigenschaften der Elektronen enthalten ist. Die Korrelationsfunktion ist eine *nicht-zufällige* Größe, die Kinetik der statistischen Prozesse charakterisierend: sie beschreibt, wie sich die Fluktuationen *im Mittel* mit der Zeit entwickeln. Eine Autokorrelationsfunktion ist eine „Memory"-Funktion, sie beschreibt das „Gedächtnis" eines Systems, d.h. beantwortet die Frage „Was bleibt von einem (in unserem Fall elektronischen) Prozess zu einem späteren Zeitpunkt erhalten?"

Die vier wichtigsten **Arten elektronischen Rauschens** sind:

Schrot-Rauschen (Schottky, 1918) – Physikalische Ursache ist die diskrete Natur der elektrischen Ladung. Für das Fluktuationsspektrum gilt:

$$S_I = 2qI$$

I: Strom, q: Ladung

Thermisches Rauschen (Johnson/Nyquist, 1927/1928) – Jeder Widerstand ist bei einer endlichen Temperatur Schwankungen unterworfen aufgrund der regellosen thermischen Bewegung der Ladungsträger.[1] Man findet:

$$S_V = 4k_B TR$$

V: Spannung, k_B: Boltzmann-Konstante, T: Temperatur, R: Widerstand

Generations-Rekombinationsrauschen – Beispiel: Die Anzahl der Ladungsträger im Leitungsband eines Halbleiters fluktuiert (durch thermische Anregungsprozesse) um genau ein Elektron. $\Rightarrow$ Der Widerstand springt dann zufällig zwischen nur zwei diskreten Werten hin und her. Diese Art des Rauschens wird auch *Telegraphenrauschen* (engl.: „*random telegraph noise*") genannt und das Spektrum ist eine Lorentz-Funktion:

$$S_V(f) \propto \tau/(1 + 4\pi^2 f^2 \tau^2)$$

f: Frequenz, τ: Zeitkonstante des G-R-Prozesses, π: Zahl

1/f-Rauschen – Die Überlagerung vieler solcher Einzelprozesse führt bei einer bestimmten Verteilung der charakteristischen Zeitkonstanten τ der Einzelprozesse zu 1/f-Rauschen. Empirisch lässt sich dieses beschreiben als (Hooge 1969):

$$S_V(f) = \gamma_H V^2/\Omega n f^\alpha \qquad \text{wobei } \alpha \approx 1$$

γ_H: Material-Konstante, Ω: Volumen der Probe, n: Ladungsträgerdichte

$N = \Omega \cdot n$: gesamte Anzahl der Ladungsträger im System

---

[1] Der Ausdruck von Johnson/Nyquist ist eine Formulierung des in der Natur allgemein gültigen Fluktuations-Dissipations-Theorems, das eine exakte Beziehung zwischen der Viskosität (Reibung) eines Systems in thermischer Umgebung und dessen (unausweichlichen) spontanen Fluktuationen angibt.

II. Bitte vergegenwärtigen Sie sich folgendes:

- Schrot- und thermisches Rauschen sind frequenzunabhängig und werden daher als „weißes Rauschen" bezeichnet.

- Das thermische Rauschen ist unabhängig von Strom und Spannung! Ein größeres Signal/Rausch-Verhältnis kann also durch einen größeren Strom durch die Probe erzielt werden (bitte selbst herleiten).

- Die spektrale Leistungsdichte des G-R-Rauschens ist ein Lorentzspektrum. Dies ergibt sich analytisch, wenn man die Autokorrelationsfunktion eines Zwei-Niveau-Systems (Doppelmuldenpotential) berechnet.

- Das 1/f-Rauschen skaliert antiproportional mit dem Volumen Ω der Probe bzw. der absoluten Anzahl der Ladungsträger $N = \Omega n$. Dadurch ist das Signal/Rausch-Verhältnis (selbst herleiten) proportional $\sqrt{N}$. 1/f-Rauschen ist also ein Problem bei immer kleiner werdenden Strukturen (Nanophysik!) sowie bei Niederfrequenz-Anwendungen.

- Das Signal/Rausch-Verhältnis für 1/f-Rauschen ist unabhängig von Strom oder Spannung, d.h. kann *nicht* durch höhere Strome verbessert werden (selbst herleiten)!

III. Weitere Anmerkungen

- Das 1/f-Rauschen tritt auf in (fast) allen Bereichen der Festkörperphysik, z.B. in Halbleitern, metallischen Filmen, Spin-Gläsern, magnetischen Tunnel-Kontakten, GMR-Sensoren (GMR: „giant magnetoresistance"; siehe Leseköpfe von magnetischen Computerfestplatten), granularen Metallen und Supraleitern, halb-

metallischen Ferromagneten, molekularen (organische) Halbleitern und Metallen, Hochtemperatursupraleitern, etc.

Gibt es also einen *universellen* Mechanismus für elektronisches 1/f-Rauschen? In der Tat sind die mikroskopischen Ursachen für viele Systeme noch weitgehend unverstanden!

- 1/f-Fluktuationen sind ebenso universell in der gesamten Natur und treten auf z.B. in der Lichtintensität von Quasaren, beim menschlichen Herzschlag, der Stärke von Erdbeben, dem Wasserstand des Nils, dem Verkehrsaufkommen auf Autobahnen, der Verteilung von Primzahlen, bei Fluktuationen in Tonhöhe und Melodie von klassischer Musik, etc. pp.   *Wie ist das zu erklären?*

- Die Varianz eines perfekten 1/f-Rauschens würde divergieren, wenn auch nur logarithmisch.

  → Es *müssen* Abschneidefrequenzen existieren! Hohe Frequenzen: endliche Streuzeiten der Ladungsträger. Tiefe Frequenzen: bisher nicht gefunden?!?

IV. Themen zur Vorbereitung – relevant im Kolloquium zu Beginn des Versuchstages und für den „Theorieteil" des Protokolls

- Arten elektronischen Rauschens und ihre Besonderheiten: thermisches Rauschen, Schrotrauschen, Generations-Rekombinationsrauschen (Telegraphen-Rauschen), 1/f-Rauschen.
- AC 4-Punkt-Widerstandsmessungen mit Lock-In-Technik
- Für Masterstudenten außerdem: AC 5-Punkt-Messung.
- Grundlagen der Physik organischer Ladungstransfersalze (molekularer Metalle)

V. Versuchsablauf

Tutorium: Grundlagen elektronisches Rauschen

1. Vertraut machen mit dem Messaufbau (Schaltbild): AC-Widerstandsmessungen mit dem Lock-In-Verstärker, Rauschmessungen mit dem Signalanalysator, Software, Datensicherung, graphische Darstellung (Origin).
2. Bestimmung des Spannungsrauschens verschiedener ohmscher Widerstände. Charakteristische Frequenzabhängigkeit? Abhängigkeit vom Strom? Vergleich mit der theoretischen Erwartung. Bestimmung der Boltzmann-Konstante aus diesen Messungen.
3. Eventuell: Abkühlen der ohmschen Widerstände. Bestimmung des Rauschspektrums bei der Siedetemperatur von Stickstoff (77K). Bestimmung der Boltzmann-Konstante aus diesen Messungen. Mit bekannter Boltzmann-Konstante (Literatur, vorherige Messung bei Raumtemperatur) wird die Temperatur bestimmt und mit der des Temperatursensors verglichen.

Tutorium: Grundlagen „niedrigdimensionale molekulare Metalle" (organische Ladungstransfersalze)

1. Elektrischer Widerstand des organischen Ladungstransfersalzes κ-(BEDT-TTF)$_2$Cu[N(CN)$_2$]Cl bei Raumtemperatur.
2. Bestimmung der spektralen Leistungsdichte der Spannungs- bzw. Widerstandsfluktuationen als Funktion des Stroms. Charakteristische Frequenzabhängigkeit? Welcher Zusammenhang besteht zwischen der spektralen Leistungsdichte und dem Strom?

VI. Hinweise zur Ausarbeitung

Ausarbeitung in Form einer wissenschaftlichen Veröffentlichung („Paper"):

Motivation → Allgemeiner Zusammenhang. Was wurde gemacht und warum?

Theorieteil → Kurze Darstellung der mathematischen Grundlagen des Rauschens. *Herleitung des Ausdrucks für das Signal-/Rausch-Verhältnis für die verschiedenen Rauscharten.*

Versuchsbeschreibung → Was haben sie experimentell wie gemacht? Skizzen!

Ergebnisse zeigen → Graphische Präsentation der Daten.

Analyse und Diskussion → **Auswertung**.

Schlussfolgerungen und Zusammenfassung → Bewertung des Experimentes. **Mögliche Fehlerquellen**.

Referenzen → Benutzte Literatur.

VII. Literatur

- Übersichtsartikel *Basic Concepts of Fluctuation Spectroscopy* (J. Müller, 2010)
- Kurze Beschreibung *What is a lock-in amplifier* (SR830 Operating Manual, Stanford Research Systems)
- Übersichtsartikel *Organic Charge Transfer Salts* (J. Müller, 2010)

Alle Materialien sind in dieser Versuchsanleitung enthalten!

VIII. Selbsttest

Wenn Sie gut vorbereitet sind, sollten Sie diese Fragen für sich selbst überzeugend beantworten und Ihrem Versuchspartner verständlich erklären können. (Dient auch zur späteren Darstellung im Versuchsprotokoll.)

1. Was sagt die spektrale Leistungsdichte einer fluktuierenden Größe aus?
2. Was ist die Ursache des thermischen Rauschens?
3. Welches einfache Modell kann 1/f-Rauschen in Halbleitern, z.B. Si-MOSFETs, erklären?
4. Was ist das Funktionsprinzip eines Lock-In-Verstärkers?
5. Wie kommt elektrische Leitfähigkeit in molekularen (organischen) Festkörpern zustande?
6. Was sind die interessanten physikalischen Eigenschaften dieser organischen Ladungstransfersalze (siehe Phasendiagramm)?

1 Basic Concepts of Fluctuation Spectroscopy

1.1 Introduction – Definitions

"Whether noise is a nuisance or a signal depends on who you ask. [...]", stated in an article by C. Beenakker and M. Schönenberger about shot noise [1], points up the fact that most people and even most physicists, consider *noise* as a nuisance, an unwanted disturbance, which limits the accuracy of a physical measurement. Some scientists, however, may consider it as a true measurement *signal*, which contains valuable information about the system that is subject to fluctuations. For example, in the fluctuations of the conductivity or resistivity there is hidden information about the dynamics and correlation of charge carriers, which is not contained in measurements of the mean quantity, i.e. the conductivity or resistivity of the sample itself. Electronic noise refers to random fluctuations in the current flowing through a material or in the voltage measured across. Noise is a random, i.e. stochastic process, but its statistical properties may be independent of time. We now give a brief overview of such *statistically stationary processes*, which can be treated in time and frequency space [2].

We consider a time-dependent physical quantity, like the voltage drop $V(t)$ across a sample, which fluctuates around its average value

$$\langle V \rangle = \lim_{T \to \infty} \frac{1}{T} \int_{-T/2}^{T/2} V(t) \mathrm{d}T, \tag{1}$$

where T is the duration of the measurement. The first statistical analysis of electronic noise often is to check whether the fluctutions are Gaussian (see also Fig. 6 below): for independent, non-interacting processes, the probability density function is given by the normal (Gaussian) distribution

$$\mathcal{P}(V) = \frac{1}{\sqrt{2\pi\sigma^2}} \exp\left[-\frac{(V - \langle V \rangle)^2}{2\sigma^2}\right], \tag{2}$$

where σ^2 is the variance defined as

$$\sigma^2 = \langle (V(t) - \langle V \rangle)^2 \rangle = \langle (\delta V)^2 \rangle = \langle V^2 \rangle - \langle V \rangle^2. \tag{3}$$

In frequency space, it is useful to ask, how much power is associated with different parts of the frequency spectrum. The Fourier transform of the voltage signal $V(t)$ is given by

$$\tilde{V}(\omega) = \int_{-\infty}^{\infty} V(t) e^{-\mathrm{i}\omega t} \mathrm{d}t. \tag{4}$$

The *power spectral density* (PSD) of the fluctuations — the quantity that is usually measured in noise experiments — can be defined as

$$S_V(\omega) = \langle |\tilde{V}(\omega)|^2 \rangle. \tag{5}$$

The units of S_V are V^2/Hz. In case of a statistically stationary process, the PSD is related to the *autocorrelation function*

$$\Psi(\tau) = \langle V(t) V(t + \tau) \rangle \tag{6}$$

through the Wiener-Khinchin theorem

$$S_V(\omega) = 4 \int_0^{\infty} \Psi(\tau) \cos \omega\tau \mathrm{d}\tau. \tag{7}$$

The autocorrelation function $\Psi(\tau)$ provides a measure of the "memory" of an electronic process, i.e. what remains from a fluctuation after a specific time interval τ. $\Psi(\tau)$ is a nonrandom characteristic of the kinetics of these random fluctuations, describing how the fluctuations — on average — evolve in time [3]. In this context, $\Psi(\tau)$ is related to the dynamics of electronic processes in solids. The inverse Fourier transform gives

$$\Psi(\tau) = \frac{1}{2\pi} \int_0^{\infty} S_V(\omega) \cos \omega\tau \mathrm{d}\omega, \tag{8}$$

which means that by measuring the PSD of a physical system, one in principle has access to the related autocorrelation function describing its microscopic properties. The autocorrelation function at zero time interval, $\Psi(\tau = 0)$, is equal to the variance of the signal, a quantity of major importance for all

scientific experiments. It is obtained, when integrating the PSD over all frequencies $f = \omega/2\pi$:

$$\langle V(t)^2 \rangle = \int\limits_0^\infty S_V(f)\mathrm{d}f \equiv \Psi(0), \quad \text{with } \langle V(t) \rangle = 0. \tag{9}$$
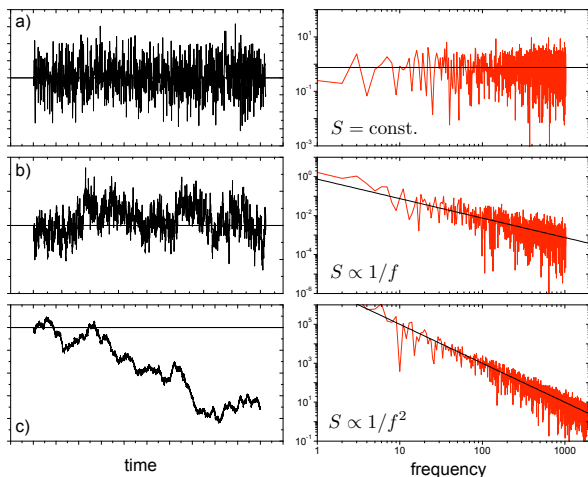

Figure 1: Time trains of different noise signals (left) and the corresponding power spectra (right). a) Sampled "white noise". The individual amplitudes are independently random values with a normal (Gaussian) distribution. This noise has a flat power spectrum. b) "Flicker noise" or $1/f$ noise. The power spectrum of this noise ($\propto 1/f$) has a divergent integral at both high and low frequencies. c) Random-walk noise with a power spectrum $\propto 1/f^2$.

Following the discussion in [4] we show in Fig. 1 computer-generated time trains of different noisy signals and the corresponding power spectra of the noise. Fig. 1 a) is an example of a totally random signal, so-called "white noise", which is familiar to almost every scientist. The most important example is thermal noise of a resistor (see Section 1.2). The name stems from the frequency-independent PSD, i.e. $S = \text{const.}$, which means that it has equal power in every unit of bandwidth, i.e. per one Hz. The power spectrum is convergent at low frequencies, but there is an infinite power at high frequencies. As

a result, as the figure suggests, thermal noise is infinitely choppy, no matter how fine a horizontal scale one chooses to look at, so the instantaneous value of the noisy signal is undefined. On the other hand, the mean value of the noise converges upon averaging over longer and longer time intervals.

In contrast, the time train shown in Fig. 1 c) — a so-called random walk — has a power spectrum $S \propto 1/f^2$, which means that the noise power is convergent if we integrate from some finite frequency to infinity. There is a finite amount of power at high frequencies, but an infinite amount of power at low frequencies. Consequently, the function does have a well-defined value at each point, but there is no mean value over long times. An important example for a random walk is the Brownian movement of small particles immersed in a fluid, which has been statistically analyzed by A. Einstein in 1905 [5, 6].

It is a striking observation, that most physical systems are neither as rough nor as smooth as these extreme cases shown in Fig. 1 a) and c), respectively, but exhibit an "intermediate" behavior like the one in Fig. 1 b). This behavior is exciting, there seems to be "something happening" on all time scales, there are both rapid fluctuations and slow general trends. The corresponding stochastic function has a spectrum $S \propto 1/f$ and hence is called $1/f$ noise, or sometimes "excess noise" or "flicker noise". It has an infinite amount of power both at high and low frequencies (see discussion below), it is a true long-term memory process and is most fascinating due to its occurrence in a large variety of different systems found in nature, like earthquakes [7], nucleotide sequences in DNA chains [8], the human heart rate [9], human cognitive processes [10], music (fluctuations of loudness and pitch in J.S. Bach's concertos [11]), astronomy (light curves of quasi-stellar objects, see [4]), and — last but not least — many condensed matter systems, see e.g. [3, 2] for an overview. One could add many more surprising systems to this list, but — although the apparent universality of $1/f$-type fluctuations is most intriguing — it is obviously questionable to compare such different complex systems. Rather there seems to be a mathematical coincidence at work, than an underlying universal law of nature.

The best studied and documented examples of $1/f$

noise are probably electronic fluctuations in solids. Before we describe such properties in low-dimensional molecular conductors, we will briefly review the most common types of noise in condensed-matter systems, including $1/f$ noise, and discuss an empirical property of the latter.

1.2 Most Common Types of Noise

In solids, electrical noise may have different origins, as e.g. defect motion, structural excitations, magnetic domains and spin fluctuations, charge carriers crossing an energy barrier, electronic traps, percolation effects or current redistribution within inhomogeneous materials [3]. These potential microscopic noise sources behave like "fluctuators", which — once activated and physically coupled to the charge carriers constituting an electrical current — induce resistance or conductance fluctuations giving rise to the electrical noise we can measure [2]. Despite the inherent randomness of fluctuations, the different phenomena may be classified regarding the frequency dependence of their PSD. The four most common types of noise in solid state physics are the following:

Thermal Noise Each resistor at a finite temperature is subject to fluctuations. Observed by J.B. Johnson in 1927 [12, 13, 14] and theoretically explained by H. Nyquist in 1928 [15], this thermal noise (also called "Johnson noise") appears in all resistors, and results from the random motion of charge carriers in equilibrium with a thermal bath. One finds for the mean square voltage noise: $\langle V^2 \rangle = 4k_B T R \Delta f$, where k_B is the Boltzmann constant, T the temperature, R the resistance of the sample, and Δf the frequency bandwidth of the measurement. The Fourier transform yields a constant noise power spectral density, thermal noise is frequency independent, "white" noise:

$$S_V(f) = 4k_B T R. \tag{10}$$

Equation(10) is a formulation of the so-called *fluctuation-dissipation theorem* [16, 17], since it relates the fluctuating noise power $\langle V^2 \rangle$ to the dissipation R in the circuit, see e.g. [18].

Shot Noise Historically, the first type of noise to be discussed was the so-called shot noise in thermionic tubes by W. Schottky in 1918 [19]. It is a non-equilibrium form of noise, originating in the discrete nature of charge carriers and related to the passage of current across an energy barrier. It has been observed in many solid state devices, such as p-n junctions, magnetic tunnel junctions, etc. The PSD of shot noise is also flat, with

$$S_I(f) = 2qI, \tag{11}$$

where q is the charge of the carriers. Measuring shot noise provides a new way of determining the elementary charge e [19], the charge of Cooper pairs in superconductors [20], as well as the quasiparticle charge in the fractional quantum Hall effect [21].

$1/f$ Noise As described above, $1/f$ noise is not only universally observed in nature, but also ubiquitous in solid state systems [22, 23, 24, 3, 25, 2]: it is found in such different systems as homogeneous semiconductors, metallic thin films, spin glasses, magnetic tunnel junctions and tunneling-magnetoresistance (TMR) devices, giant-magnetoresistance (GMR) devices and colossal magnetoresistance (CMR) materials, granular metals and superconductors, half-metallic ferromagnets, etc. Again, it is tempting to speculate about a common origin of the $1/f$-type fluctuation properties. A phenomenological approach by F.N. Hooge in 1969 [26] led to an empirical formula for $1/f$ voltage fluctuations

$$S_V(f) = \frac{\gamma_H V^2}{N_c f^\alpha}, \tag{12}$$

where $N_c = n_c \Omega$ is the number of charge carriers in the noise volume Ω of a sample with carrier concentration n_c, and γ_H a parameter (Hooge's constant) characterizing the noise level of the system. In the noise literature, frequency exponents $0.8 \leq \alpha \leq 1.4$ are considered to describe "$1/f$ noise". For $\alpha = 1$, γ_H is dimensionless. A theoretical motivation of the Hooge parameter — initially assumed to be equal to 2×10^{-3} — was not possible; in particular, γ_H may strongly depend on temperature and over the years was found to vary over many orders of magnitude

from 10^{-6} to 10^7 for different systems [2]. Despite these strong arguments against a physical meaning of γ_H, Hooge's equation is a convenient way to compare different systems and to provide an estimate of how noisy a device is at room temperature.

Because $1/f$ noise scales inversely with the size of the system under investigation, it is on the one hand a big obstacle for miniaturization of devices for application in information and sensing technology! On the other hand, Eq. (12) suggests that decreasing the volume, e.g. by fabricating a material as a thin film, may allow for measuring the intrinsic $1/f$ noise properties even of "quite" materials with small values of γ_H or of good metals having a high carrier concentration n_c.

Another important aspect refers to the fact that for pure $1/f$ noise, the noise power diverges on both ends when integrating to very low and very high frequencies, cf. the discussion of Fig. 1. Thus, neither the instantaneous value of the signal nor the long-time mean of the measurement is well-defined. This noise is scale invariant in a way that each logarithmic interval contributes the same power. This, however, means that the divergence is only logarithmic, and thus very weak: a fluctuating system being observed with a frequency related to the shortest conceivable time interval (time light travels the distance of the diameter of a proton) over the longest conceivable time period (age of the universe) — covering roughly 40 decades — would dissipate only a few times more noise power than a half-day experiment in a laboratory!
Still, a diverging variance is unphysical, so frequency limits must exist. A *high-frequency cut-off* for resistance noise measurements in solids is naturally given due to the finite scattering time of electrons and by the frequency above which the $1/f$ noise sinks below the white background noise level. In practice, a *low-frequency cut-off*, which necessarily yields a finite experimental value of the fluctuation variance, is given by the stability of the experiment and the patience of the experimentalist. Theoretically, an intrinsic low-frequency cut-off also should be present. In this respect, it is interesting to note that measurements of semiconductor noise sources (operational amplifiers) by M.A. Caloyannides revealed a $1/f$-like

PSD down to a measurement frequency of $10^{-6.3}$ Hz [27], which requires averaging times of the order of several weeks! It remains an open problem to explain long-term memory correlations down to such low frequencies.

Generation-Recombination Noise Very important in condensed matter systems is generation-recombination noise. A prime example is a semiconductor, where electrons are excited into the conduction band creating electron-hole pairs, which later recombine. If only one electron was excited, i.e. the number of electrons in the conduction band was modified just by one, then the resistance would change in discrete steps between two values leading to a so-called "random telegraph signal" (RTS). This random telegraph noise (RTN) is of non-Gaussian type. For Gaussian noise, the system is fully described by the lowest-order correlation function $\Psi(\tau)$, Eqs. (6) and (8). The lack of Gaussianity, however, requires the use of higher-order correlation functions. This may be caused (i) by a very small number of independent events, i.e. if only a few fluctuators (or in the extreme case: just one) couple(s) more strongly to the resistivity than others, or (ii) if the fluctuators cannot be considered as independent but rather interact with each other. Experimentally, one can access the second order correlation function $\Psi^{(2)}(\tau) = \langle V^2(t)V^2(t+\tau)\rangle$ for instance by measuring the spectrum of fluctuations in the noise power within the frequency bandwidth of the ordinary spectrum. The corresponding spectral density is called the "second spectrum", see e.g. [28, 29, 30, 31].
The (lowest-order) autocorrelation function $\Psi(\tau)$ of a two-level system as shown in Fig. 2 has been calculated by S. Machlup [32]. The PSD of an RTS caused by switching events between two states with voltage amplitude ΔV and characteristic lifetimes τ_1 and τ_2 is given by a Lorentzian:

$$S_V(f) = \frac{4(\Delta V)^2}{\tau_1 + \tau_2} \cdot \frac{1}{(1/\tau_c)^2 + (2\pi f)^2}, \qquad (13)$$

where $1/\tau_c = 1/\tau_1 + 1/\tau_2$. Fig. 2 c) shows that the spectrum is flat for low frequencies (no "memory" for long times $t \gg \tau_c$, cf. white noise shown in Fig. 1 a)

4

and falls off like $1/f^2$ (full time-correlation for $t \ll \tau_c$, cf. random walk in Fig. 1 c). The corner frequency $f_c = 1/2\pi\tau_c$ is related to the characteristic time constants of the system, which can directly be measured through the PSD. The statistical study of lifetimes in the different states provides extremely rich information on the dynamics and the energy scales of the switching events as well as the related electronic properties, see e.g. [33, 34] and references therein for recent lifetime-studies of defects in semiconductor heterostructures.
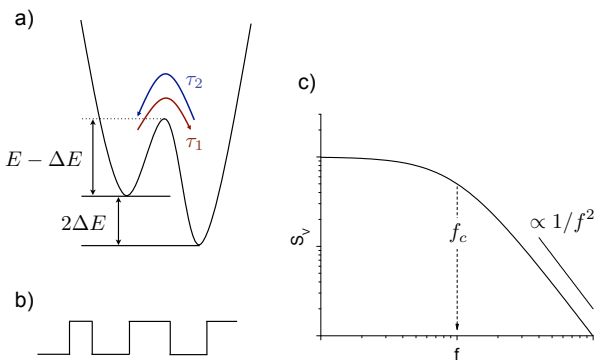

Figure 2: A fluctuating two-level system. a) Model double-well potential with characteristic energies and time constants. b) Random telegraph noise in the time domain. c) Corresponding Lorentzian spectrum in the frequency domain. See [2, 35].

As will be discussed below in more detail, a possible mechanism for $1/f$ noise is the superposition of a large number of independent Lorentzian spectra with a proper distribution of characteristic lifetimes [36, 37, 38]:

$$S(f) \propto \int D(\tau) \frac{\tau}{1 + 4\pi^2\tau^2 f^2} \mathrm{d}\tau, \qquad (14)$$

where τ is the characteristic time constant of a Lorentzian spectrum and $D(\tau)$ is the distribution function of τ. Accordingly, the first theoretical model for $1/f$ noise in semiconductors by A.L. McWhorter [39] assumes a homogeneous distribution of traps in the oxide layer of Si-MOSFET devices, from which electrons tunnel into the conducting channel, corresponding to a distribution of average lifetimes of

the trap states consistent with the observed 1/ noise. Here, assuming that the characteristic lifetimes exponentially decay with distance from the conducting channel, a homogeneous spatial distribution of traps leads to $D(\tau) \propto 1/\tau$ and $S \propto 1/f$ when integrating 14.

1.3 Experimental Realization

For low-frequency measurements of conducting samples with resistance values below about $10 - 100\,\mathrm{k\Omega}$, an ac technique is best suited. A schematic diagram of the experimental setup is shown in Fig. 3. The five-terminal setup, where the sample is placed in a Wheatstone bridge in order to suppress the constant voltage offset, is designed to avoid the influence of fluctuations in external sources, such as the voltage source, the bath temperature, or applied magnetic field [40]. The bridge type design makes the output of the circuit insensitive to these fluctuations. The noise signal is preamplified, where one tries to match the input impedance and excitation frequency in or close to the "eye" of the preamplifier's noise figure in order to reduce the amount of noise added by the preamplifier above the thermal noise. Usually, the operating frequency of the preamplifier is shifted to an ac excitation frequency of $f_0 \sim 10^2 - 10^3$ Hz. With an ac current $I = I_0 \sin(2\pi f_0 t)$, the resistance fluctuations modulate the sinusoidally excited carriers to produce noise sidebands, which can be demodulated by a phase-sensitive detector (lock-in amplifier). The
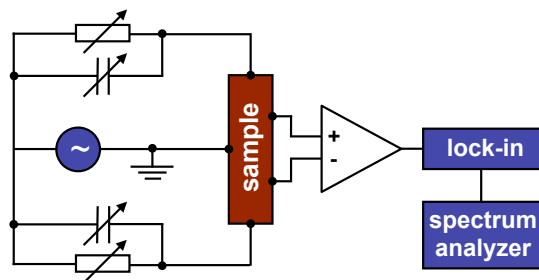

Figure 3: Five-terminal ac setup for measuring resistance fluctuations [40]. After [35].

output signal of the lock-in amplifier is then processed into a spectrum analyzer, the function of which is described below (see Fig. 5). The PSD of the lock-ins output is given by

$$S_V(f) = G_0^2[S_V^0(f_0 - f) + (I_0^2/2)S_R(f)\cos\delta], \quad (15)$$

where G_0 is the gain of lock-in, defined to be the ratio of the dc output voltage to the rms ac voltage at the input, and δ is the detection phase angle relative to the excitation current. The validity of Eq. (15) is limited to $f < f_0/2$. In practice, f is chosen to be at least one order of magnitude smaller than the carrier frequency f_0. The floor (background) noise is $S_V^0(f_0 - f) \approx S_V(f_0)$, so it is particularly suitable for low-frequency noise measurements. Proper impedance matching and choice of excitation frequency allow the noise to be measured down to 10^{-3} Hz. For more insulating samples with resistances larger than $10 - 100\,\mathrm{k\Omega}$, a dc technique (with a similar setup) can be used, which allows to measure up to higher frequencies.

Johnson and shot noise correspond to the lowest noise level one may expect in a material or a device. The former provides a direct calibration of an electronic transport experiment, as the background noise, in zero current, must tend to the thermal noise of the sample. The noise level above the theoretical thermal noise is due to the electronic setup, impedance mismatch and inefficient shielding and grounding of the experiment [2]. Care must be taken to rule out or eliminate spurious noise sources, especially those coming from the electrical contacts. The observed noise spectra need to be independent of the lock-in amplifier, its driving frequency, and the preamplifier as long as the conditions for proper impedance matching are met. In the ac circuit, the 90° degrees phase-shifted (y-channel) signal is expected to show frequency-independent "white" noise and — representing the noise floor of the experimental setup — and may be subtracted from the x-channel signal, a technique which sometimes allows to extend the accessible frequency range to higher values. Figure 4 shows measurements of voltage noise PSDs of an organic conductor [41, 42] taken at diffferent bias currents I. Since one expects that $S_V/V^2 = S_R/R^2$, where S_V and S_R are the voltage and resistance noise
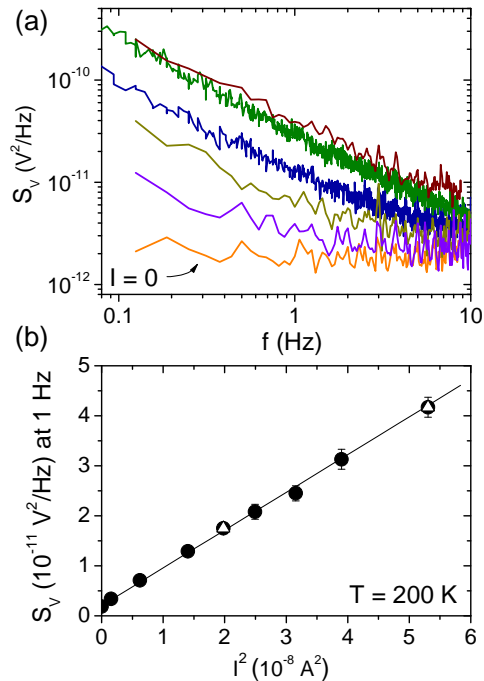

Figure 4: a) Voltage noise power spectral density $S_V(f)$ for different bias currents I of an organic conductor at $T = 200\,\mathrm{K}$. For $I = 0$, we observe a "white" floor noise spectrum. b) Scaling behavior of $S_V(f = 1\,\mathrm{Hz})$ with bias currents I. The line is a linear fit to the data in the representation S_V vs. I^2. Open triangles represent spectra obtained for a different value of the current limiting resistor r yielding an identical scaling behavior.

PSDs, respectively, a necessary condition for checking if the measured noise indeed is solely due to resistance fluctuations of the sample is a scaling behavior $S_V \propto I^2$. The data in Fig. 4 show an excellent scaling. Also, as expected and required, the observed scaling is independent of the ratio R/r, where R is the sample resistance and r is the value of the current-limiting resistor in the bridge circuit. Furthermore, as shown in the inset, a white floor noise spectrum (x-channel signal) is observed for $I \to 0$.

The above-described concepts and the experimental setup are schematically depicted and summarized
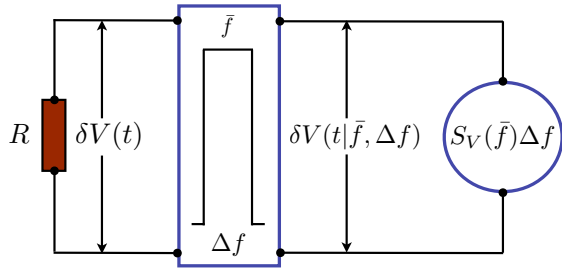
Figure 5: Schematic diagram of a spectral analyzer for measuring the spectral density of resistance noise. Its functions are described in the text. After [3].

in Figs. 5 and 6. The "heart" of the experiment is a signal analyzer (Fig. 5, for simplicity the amplification of the signal is not shown here). The source of noise is the sample resistance R, so we measure a time-dependent voltage drop $\delta V(t)$ across the resistor. A representative real-time measurement of a sample and the histogram of the voltage amplitudes are shown in Fig. 6 a) and b), respectively. Note that the noise is Gaussian, i.e. the corresponding $1/f$-type spectrum shown in Fig. 6 c) may be caused by a superposition of a large number of independent fluctuators. The spectrum analyzer, as schematically depicted in Fig. 5, contains a band-pass adjustable frequency filter with a narrow bandwidth Δf and a central frequency $\bar{f}$, and an output detector that responds to the mean square of the signal: $\delta V(t|\bar{f}, \Delta f)$ is the output (filtered signal) and $\langle [\delta V(t|\bar{f}, \Delta f)]^2 \rangle \equiv S_V(\bar{f})\Delta f$ is the power of the filtered signal. Technically, the spectral analyzer transforms the time train into the frequency domain by performing a real-time Fourier transformation of the signal, so the setup allows for averaging the obtained spectra to gain a higher resolution. A convenient compromise between resolution and measurement time is to take about 50 averages for each frequency octave. For the final spectrum at a given temperature, the averaged spectra for different octaves are put together.

In summary, the role of the noise spectrum analyzer processing the preamplified signal may be viewed as similar to the role of a microscope: it
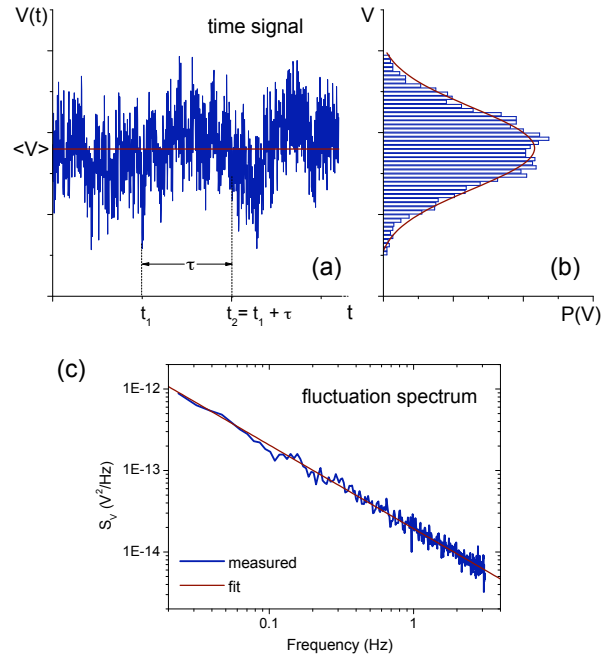

Figure 6: a) Real-time measurement of a noise signal, as e.g. the voltage drop across a sample $V(t)$ (*input*). b) Histogram of $V(t)$, which can be fitted to a normal (Gaussian) probability distribution, Eq. (2). c) Corresponding power spectrum in the frequency domain (*output*) showing a $1/f^\alpha$ characteristics with $\alpha \simeq 1$.

enables one to visualize the microscopic motion and transitions of particles [3].

Extracted from *Fluctuation Spectroscopy — A new Approach to Study Electronic Correlations in Organic Molecular Materials* by J. Müller.

References

[1] C. Beenakker and C. Schönenberger. *Physics Today*, 56:37, 2003.

[2] B. Raquet. *Spin Electronics*, chapter Electronic Noise in Magnetic Materials and Devices, pages 232 – 273. M. Ziese, M. J. Thornton, Ed., Springer, Berlin Heidelberg, 2001.

[3] Sh. Kogan. *Electronic Noise and Fluctuations in Solids.* Cambridge University Press, New York, 1996.

[4] W.H. Press. *Comments Astrophys.*, 7:103, 1978.

[5] A. Einstein. *Ann. Phys.*, 17:549, 1905.

[6] A. Einstein. *Ann. Phys.*, 19:289,371, 1906.

[7] P. Bak, K. Christensen, L. Danon, and T. Scanlon. *Phys. Rev. Lett.*, 88:178501, 2002.

[8] C.-K. Peng, S.V. Buldyrev, A.L. Goldberger, S. Havlin, F. Sciortino, M. Simons, and H.E. Stanley. *Nature*, 356:168, 1992.

[9] C.-K. Peng, J. Mietus, J.M. Hausdorff, S. Havlin, H.E. Stanley, and A.L. Goldberger. *Phys. Rev. Lett.*, 70:1343, 1993.

[10] D.L. Gilden. *Psychological Review*, 108:33, 2001.

[11] R.V. Voss and J. Clarke. *Nature*, 258:317, 1997.

[12] J.B. Johnson. *Nature*, 119:50, 1927.

[13] J.B. Johnson. *Phys. Rev.*, 29:367, 1927.

[14] J.B. Johnson. *Phys. Rev.*, 32:97, 1928.

[15] H. Nyquist. *Phys. Rev.*, 32:110, 1928.

[16] H.B. Callen and T.A. Welton. *Phys. Rev.*, 83:34, 1951.

[17] J. Weber. *Phys. Rev.*, 101:1620, 1956.

[18] S.J. Blundell and K.M. Blundell. *Concepts in Thermal Physics.* Oxford University Press, New York, 2nd edition, 2010.

[19] W. Schottky. *Ann. Phys.*, 57:541, 1918.

[20] F. Lefloch, C. Hoffmann, M. Sanquer, and D. Quirion. *Phys. Rev. Lett.*, 90:067002, 2003.

[21] L. Saminadayar, D.C. Glattli, Y. Jin, and B. Etienne. *Phys. Rev. Lett.*, 79:2526, 1997.

[22] P. Dutta and P.M. Horn. *Rev. Mod. Phys.*, 53:497, 1981.

[23] M.B. Weissman. *Rev. Mod. Phys.*, 60:537, 1988.

[24] M.B. Weissman. *Rev. Mod. Phys.*, 65:4829, 1993.

[25] B. Raquet, J.M.D. Coey, S. Wirth, and S. von Molnár. *Phys. Rev. B*, 59:12435, 1999.

[26] F.N. Hooge. *Phys. Lett.*, A 29:139, 1969.

[27] M.A. Caloyannides. *J. Appl. Phys.*, 45:307, 1973.

[28] M.B. Weissman, N.E. Israeloff, and G.B. Alers. *J. Magn. Magn. Mat.*, 114:87, 1992.

[29] G.T. Seidler and S.A. Solin. *Phys. Rev. B*, 53:9753, 1996.

[30] K.M. Abkemeier. *Phys. Rev. B*, 55:7005, 1997.

[31] G.M. Khera and J. Kakalios. *Phys. Rev. B*, 56:1918, 1997.

[32] S. Machlup. *J. Appl. Phys.*, 25:341, 1954.

[33] J. Müller, S. von Molnár, Y. Ohno, and H. Ohno. *Phys. Rev. Lett.*, 96:186601, 2006.

[34] J. Müller, Y.Q. Li, S. von Molnár, Y. Ohno, and H. Ohno. *Phys. Rev. B*, 74:125310, 2006.

[35] Y.Q. Li. *Optimization of Hall magnetometry and single magnetic nanoparticle measurements.* Phd thesis, Florida State University, Tallahassee, FL, 2003.

[36] J. Bernamont. *Ann. Phys.*, 7:71, 1937.

[37] F.K. Du Pré. *Phys. Rev.*, 78:615, 1050.

[38] A. Van Der Ziel. *Physica*, 16:359, 1050.

[39] A.L. McWhorter. *Semiconductor Surface Physics*, page 207. R.H. Kingston, Ed., University of Pennsylvania Press, Philadelphia, 1957.

[40] J.H. Scofield. *Rev. Sci. Instr.*, 58:985, 1987.

[41] J. Müller, J. Brandenburg, and J.A. Schlueter. *Phys. Rev. Lett.*, 102:047004, 2009.

[42] J. Müller, J. Brandenburg, and J.A. Schlueter. *Phys. Rev. B*, 79:214521, 2009.

WHAT IS A LOCK-IN AMPLIFIER?

Lock-in amplifiers are used to detect and measure very small AC signals - all the way down to a few nanovolts! Accurate measurements may be made even when the small signal is obscured by noise sources many thousands of times larger.

Lock-in amplifiers use a technique known as phase-sensitive detection to single out the component of the signal at a specific reference frequency AND phase. Noise signals at frequencies other than the reference frequency are rejected and do not affect the measurement.

Why use a lock-in?
Let's consider an example. Suppose the signal is a 10 nV sine wave at 10 kHz. Clearly some amplification is required. A good low noise amplifier will have about 5 nV/$\sqrt{\text{Hz}}$ of input noise. If the amplifier bandwidth is 100 kHz and the gain is 1000, then we can expect our output to be 10 µV of signal (10 nV x 1000) and 1.6 mV of broadband noise (5 nV/$\sqrt{\text{Hz}}$ x $\sqrt{100}$ kHz x 1000). We won't have much luck measuring the output signal unless we single out the frequency of interest.

If we follow the amplifier with a band pass filter with a Q=100 (a VERY good filter) centered at 10 kHz, any signal in a 100 Hz bandwidth will be detected (10 kHz/Q). The noise in the filter pass band will be 50 µV (5 nV/$\sqrt{\text{Hz}}$ x $\sqrt{100}$ Hz x 1000) and the signal will still be 10 µV. The output noise is much greater than the signal and an accurate measurement can not be made. Further gain will not help the signal to noise problem.

Now try following the amplifier with a phase-sensitive detector (PSD). The PSD can detect the signal at 10 kHz with a bandwidth as narrow as 0.01 Hz! In this case, the noise in the detection bandwidth will be only 0.5 µV (5 nV/$\sqrt{\text{Hz}}$ x $\sqrt{.01}$ Hz x 1000) while the signal is still 10 µV. The signal to noise ratio is now 20 and an accurate measurement of the signal is possible.

What is phase-sensitive detection?
Lock-in measurements require a frequency reference. Typically an experiment is excited at a fixed frequency (from an oscillator or function generator) and the lock-in detects the response from the experiment at the reference frequency. In the diagram below, the reference signal is a square wave at frequency ω_r. This might be the sync output from a function generator. If the sine output from the function generator is used to excite the experiment, the response might be the signal waveform shown below. The signal is $V_{sig}\sin(\omega_r t + \theta_{sig})$ where V_{sig} is the signal amplitude.

The SR830 generates its own sine wave, shown as the lock-in reference below. The lock-in reference is $V_L\sin(\omega_L t + \theta_{ref})$.
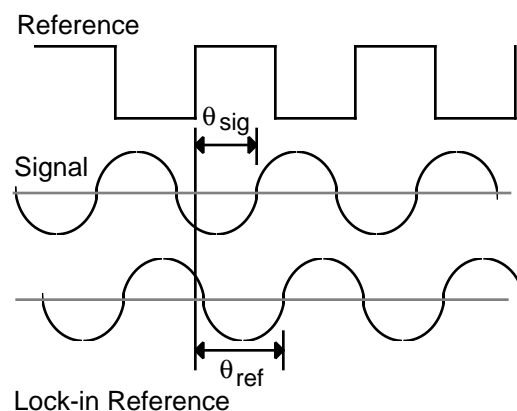
Lock-in Reference

The SR830 amplifies the signal and then multiplies it by the lock-in reference using a phase-sensitive detector or multiplier. The output of the PSD is simply the product of two sine waves.

$$V_{psd} = V_{sig}V_L\sin(\omega_r t + \theta_{sig})\sin(\omega_L t + \theta_{ref})$$

$$= 1/2\ V_{sig}V_L\cos([\omega_r - \omega_L]t + \theta_{sig} - \theta_{ref}) - 1/2\ V_{sig}V_L\cos([\omega_r + \omega_L]t + \theta_{sig} + \theta_{ref})$$

The PSD output is two AC signals, one at the difference frequency ($\omega_r - \omega_L$) and the other at the sum frequency ($\omega_r + \omega_L$).

If the PSD output is passed through a low pass filter, the AC signals are removed. What will be left? In the general case, nothing. However, if ω_r equals ω_L, the difference frequency component will be a DC signal. In this case, the filtered PSD output will be

$$V_{psd} = 1/2\ V_{sig}V_L\cos(\theta_{sig} - \theta_{ref})$$

This is a very nice signal - it is a DC signal proportional to the signal amplitude.

Narrow band detection

Now suppose the input is made up of signal plus noise. The PSD and low pass filter only detect signals whose frequencies are very close to the lock-in reference frequency. Noise signals at frequencies far from the reference are attenuated at the PSD output by the low pass filter (neither $\omega_{noise}-\omega_{ref}$ nor $\omega_{noise}+\omega_{ref}$ are close to DC). Noise at frequencies very close to the reference frequency will result in very low frequency AC outputs from the PSD ($|\omega_{noise}-\omega_{ref}|$ is small). Their attenuation depends upon the low pass filter bandwidth and roll-off. A narrower bandwidth will remove noise sources very close to the reference frequency, a wider bandwidth allows these signals to pass. The low pass filter bandwidth determines the bandwidth of detection. Only the signal at the reference frequency will result in a true DC output and be unaffected by the low pass filter. This is the signal we want to measure.

Where does the
lock-in reference come from?

We need to make the lock-in reference the same as the signal frequency, i.e. $\omega_r = \omega_L$. Not only do the frequencies have to be the same, the phase between the signals can not change with time, otherwise $\cos(\theta_{sig} - \theta_{ref})$ will change and V_{psd} will not be a DC signal. In other words, the lock-in reference needs to be phase-locked to the signal reference.

Lock-in amplifiers use a phase-locked-loop (PLL) to generate the reference signal. An external reference signal (in this case, the reference square wave) is provided to the lock-in. The PLL in the lock-in locks the internal reference oscillator to this external reference, resulting in a reference sine wave at ω_r with a fixed phase shift of θ_{ref}. Since the PLL actively tracks the external reference, changes in the external reference frequency do not affect the measurement.

All lock-in measurements
require a reference signal.

In this case, the reference is provided by the excitation source (the function generator). This is called an external reference source. In many situations, the SR830's internal oscillator may be used instead. The internal oscillator is just like a function generator (with variable sine output and a TTL sync) which is always phase-locked to the reference oscillator.

Magnitude and phase

Remember that the PSD output is proportional to $V_{sig}\cos\theta$ where $\theta = (\theta_{sig} - \theta_{ref})$. θ is the phase difference between the signal and the lock-in reference oscillator. By adjusting θ_{ref} we can make θ equal to zero, in which case we can measure V_{sig} ($\cos\theta=1$). Conversely, if θ is 90°, there will be no output at all. A lock-in with a single PSD is called a single-phase lock-in and its output is $V_{sig}\cos\theta$.

This phase dependency can be eliminated by adding a second PSD. If the second PSD multiplies the signal with the reference oscillator shifted by 90°, i.e. $V_L\sin(\omega_L t + \theta_{ref} + 90°)$, its low pass filtered output will be

$$V_{psd2} = 1/2\ V_{sig}V_L\sin(\theta_{sig} - \theta_{ref})$$

$$V_{psd2} \sim V_{sig}\sin\theta$$

Now we have two outputs, one proportional to $\cos\theta$ and the other proportional to $\sin\theta$. If we call the first output X and the second Y,

$$X = V_{sig}\cos\theta \qquad Y = V_{sig}\sin\theta$$

these two quantities represent the signal as a vector relative to the lock-in reference oscillator. X is called the 'in-phase' component and Y the 'quadrature' component. This is because when $\theta=0$, X measures the signal while Y is zero.

By computing the magnitude (R) of the signal vector, the phase dependency is removed.

$$R = (X^2 + Y^2)^{1/2} = V_{sig}$$

R measures the signal amplitude and does not depend upon the phase between the signal and lock-in reference.

A dual-phase lock-in, such as the SR830, has two PSD's, with reference oscillators 90° apart, and can measure X, Y and R directly. In addition, the phase θ between the signal and lock-in reference, can be measured according to

$$\theta = \tan^{-1}(Y/X)$$

WHAT DOES A LOCK-IN MEASURE?

So what exactly does the SR830 measure? Fourier's theorem basically states that any input signal can be represented as the sum of many, many sine waves of differing amplitudes, frequencies and phases. This is generally considered as representing the signal in the "frequency domain". Normal oscilloscopes display the signal in the "time domain". Except in the case of clean sine waves, the time domain representation does not convey very much information about the various frequencies which make up the signal.

What does the SR830 measure?

The SR830 multiplies the signal by a pure sine wave at the reference frequency. All components of the input signal are multiplied by the reference simultaneously. Mathematically speaking, sine waves of differing frequencies are orthogonal, i.e. the average of the product of two sine waves is zero unless the frequencies are EXACTLY the same. In the SR830, the product of this multiplication yields a DC output signal proportional to the component of the signal whose frequency is exactly locked to the reference frequency. The low pass filter which follows the multiplier provides the averaging which removes the products of the reference with components at all other frequencies.

The SR830, because it multiplies the signal with a pure sine wave, measures the single Fourier (sine) component of the signal at the reference frequency. Let's take a look at an example. Suppose the input signal is a simple square wave at frequency f. The square wave is actually composed of many sine waves at multiples of f with carefully related amplitudes and phases. A 2V pk-pk square wave can be expressed as

$S(t) = 1.273\sin(\omega t) + 0.4244\sin(3\omega t) + 0.2546\sin(5\omega t) + ...$

where $\omega = 2\pi f$. The SR830, locked to f will single out the first component. The measured signal will be $1.273\sin(\omega t)$, not the 2V pk-pk that you'd measure on a scope.

In the general case, the input consists of signal plus noise. Noise is represented as varying signals at all frequencies. The ideal lock-in only responds to noise at the reference frequency. Noise at other frequencies is removed by the low pass filter following the multiplier. This "bandwidth narrowing" is the primary advantage that a lock-in amplifier provides. Only inputs at frequencies at the reference frequency result in an output.

RMS or Peak?

Lock-in amplifiers as a general rule display the input signal in Volts RMS. When the SR830 displays a magnitude of 1V (rms), the component of the input signal at the reference frequency is a sine wave with an amplitude of 1 Vrms or 2.8 V pk-pk.

Thus, in the previous example with a 2 V pk-pk square wave input, the SR830 would detect the first sine component, $1.273\sin(\omega t)$. The measured and displayed magnitude would be 0.90 V (rms) ($1/\sqrt{2}$ x 1.273).

Degrees or Radians?

In this discussion, frequencies have been referred to as f (Hz) and ω ($2\pi f$ radians/sec). This is because people measure frequencies in cycles per second and math works best in radians. For purposes of measurement, frequencies as measured in a lock-in amplifier are in Hz. The equations used to explain the actual calculations are sometimes written using ω to simplify the expressions.

Phase is always reported in degrees. Once again, this is more by custom than by choice. Equations written as $\sin(\omega t + \theta)$ are written as if θ is in radians mostly for simplicity. Lock-in amplifiers always manipulate and measure phase in degrees.

1 Low-Dimensional Molecular Metals

1.1 Introduction

The science of conducting organic (molecular) materials is driven by the joint efforts of chemists, materials scientists and physicists to create new classes of materials and to understand their exotic properties, see e.g. [1, 2, 3, 4] for an overview. A key feature of the materials discussed in this review is their composition of molecular building blocks and the formation of charge-transfer complexes: an electron-rich donor molecule D with a sufficiently low ionization energy is oxidized by an acceptor A having the appropriate electron affinity. This charge transfer leaves behind partially-filled molecular orbitals. When forming a crystalline solid $D_m A_n$ (m, n are integers), the constituent molecules are packed rather densely, such that the orbitals of adjacent molecules overlap, allowing the carriers to delocalize throughout the crystal.* Naturally, their electronic properties are low dimensional: owing to the strongly directional-dependent chemical bonds, significant electronic interactions may develop only along certain directions. The combination of low dimensionality with other parameters specific to molecular conductors sets the stage for Coulomb correlation effects to become relevant and, under certain circumstances, to dominate the properties of the π-electron system. These effects, together with a strong coupling of the carriers to the lattice vibrations give rise to a rich phenomenology of ground states, as e.g., magnetic and non-magnetic insulating states, correlated metallic phases and superconductivity. Other interesting phases observed are charge-ordered, Peierls and spin-Peierls, as well as charge- and spin-density-wave states. Studies of these materials have offered the exciting possibility for testing fundamental concepts of theoretical physics which were formerly only considered to be of academic interest.

What is striking about the electronic correlations arises from the fact that calculations of the electronic band structure based on standard quantum-chemical tight-binding methods (e.g. extended Hückel approximation) predict whole series of systems based on specific donor molecules to be metallic, whereas the actual ground state of some members of the series is found to be insulating. Thus, in order to understand the diversity of behaviors, the joint effects of strong electron-electron repulsion and low dimensionality have to be taken into account. In this context, a particularly interesting feature is the so-called Mott insulating state, where a gap in the charge carrying excitations opens due to electron-electron interactions. In the proximity of the Mott insulating state, which, depending on the degree of frustrating interactions, may show long-range antiferromagnetic order or remain a disordered spin liquid at low temperatures, correlated metallic phases, charge ordering and superconductivity are observed. Recent achievements from both the experimental and theoretical sides indicate that, indeed, these molecular materials provide excellent model systems for exploring the fascinating physics expected near the Mott transition.

1.2 Basic Concepts and Structural Properties

1.2.1 Charge Transfer and Molecular Orbitals

Like for any conductor, in organic materials the prerequisites of metallic behavior are the existence of charge carriers and their delocalization throughout the crystal. As mentioned above, carriers are created by a transfer of charge from a donor molecule D to an electron acceptor A. Meanwhile, organic chemistry provides an enormous number of different donor molecules, the most important of which are the tetrachalcogenafulvalenes derivatives TMTSF, TMTTF, BEDT-TTF (commonly abbreviated as ET), and BEDT-TSF (BETS), furnishing organic superconductors[†]; these and some other selected molecules are

---

*These charge-transfer salts are to be distinguished from other classes of molecular conductors such as conjugated polymers or graphite, where the conductivity comes about due to the π-electron system of the extended molecule. For the systems discussed here, an intermolecular process leads to the motion of π-carriers.

[†]TMTSF, TMTTF, BEDT-TTF, and BEDT-TSF stands for bis(tetramethyl)-tetraselenafulvalene, bis(tetramethyl)-
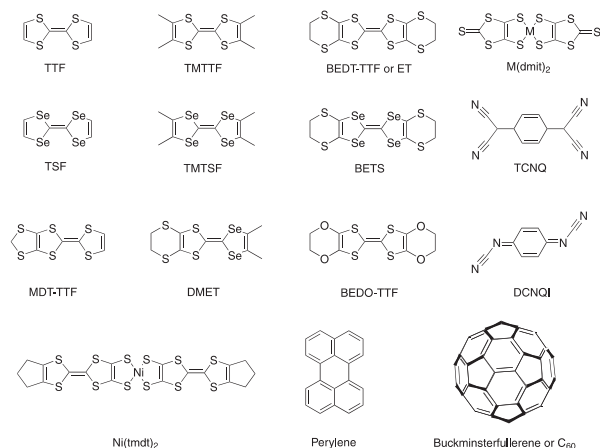
shown in Fig. 1.

Figure 1: Selected molecules that furnish organic conductors. Reprinted with permission from [3]. Copyright (2007), Springer.

The combination of a donor molecule D, as e.g. TMTSF or BEDT-TTF, with an acceptor molecule A, which may be organic or inorganic, leads to the formation of a crystalline compound D_mA_n. In the vast majority of D_mA_n salts, the donor-acceptor molecular ratio $m : n$ is fixed to $2 : 1$, i.e., two donor molecules transfer one electron to the acceptor. For these materials, the number of mobile carriers is determined by the charge transfer and independent of temperature.[‡] Upon forming the crystal, the transferred electron stays localized on the acceptor site, where a closed-shell configuration is adopted. Hence, it doesn't contribute to the electronic properties. On the donor site, however, the charge transfer leaves behind partially-filled molecular orbitals.

These molecular orbitals are obtained by taking a linear combination of atomic s- and p-orbitals of the constituent atoms, resulting in σ- and π-orbitals. While the σ-orbitals are localized along the bonding axis of adjacent atoms, having a nonzero momentum

only along this axis (parallel to the molecular plane), the π-orbitals are extended normal to the bonding plane, see Fig. 2. Due to the lower binding energy of the π-electrons compared to that of the σ-electrons, they tend to delocalize and can be easily excited. As a consequence, the carriers transferred from the donor to the acceptor have a dominantly π-electron character leaving behind a fraction $+\delta$ of π-holes per donor molecular unit D_m. The transfer of charge in the $2 : 1$ salts D_2A based on TMTSF, TMTTF, ET and BETS is experimentally found to be $\delta = 1$, see e.g. [3]. The remaining hole becomes delocalized due to a stacking arrangement of the donor molecules, which leads to an overlap of the orbitals of adjacent molecules, allowing the π-hole to propagate along the stacking direction, see Fig. 2.
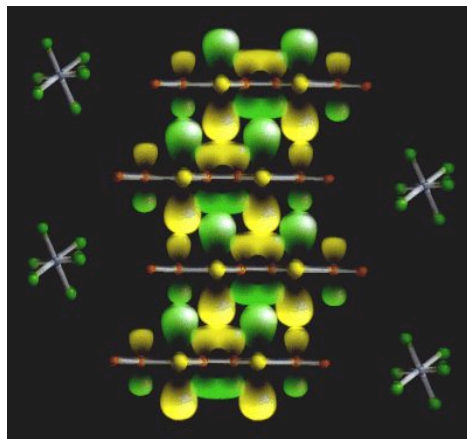

Figure 2: Schematics showing the π-molecular orbitals of TMTSF, within the crystal structure of $(TMTSF)_2PF_6$, cf. Fig. 4. The axis of highest conductivity is the stacking a-direction, where the molecular orbitals' overlap is largest. Reproduced with permission from [6]. Copyright (1998), IOP.

The building-block composition results in a distinct anisotropy of the crystal structures which is reflected in highly anisotropic Fermi surfaces and related physical properties, as e.g. electrical transport. The arrangement of molecular building blocks is schematically illustrated in Fig. 3: the building

tetrathiafulvalene, bis(ethylenedithio)-tetrathiafulvalene, and, bis(ethylenedithio)-tetraselenafulvalene, respectively.

[‡]This is in contrast to the creation of free carriers by doping a system with impurities as in the well-known example polyacetylene $(CH)_x$.

blocks are the blue and red donor and acceptor molecules, respectively, in the 2 : 1 stoichiometry. The donor molecules are represented by flat, sheet-like units, where the π-orbitals would be directed perpendicular to the molecules' planes. For a possible stacking arrangement with blocky anions, shown on the left, it is intuitively clear that the conductivity will be highest along the stacking z-axis, intermediate along y- and lowest along the x-direction, leading to quasi-1D electronic properties, cf. Figs. 2 and 4. More extended donor molecules may combine with
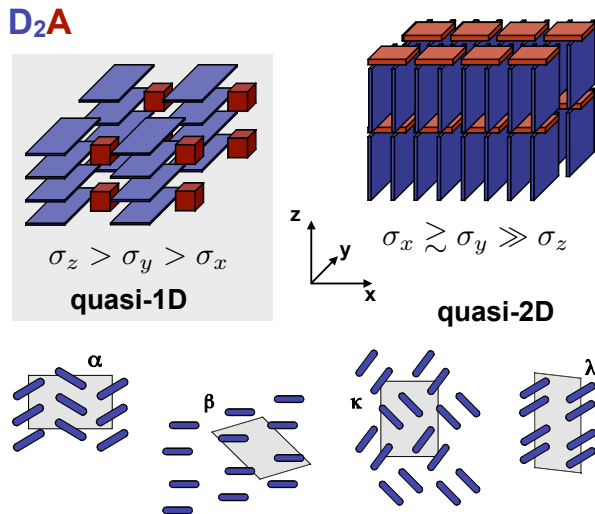

Figure 3: Schematic illustration of the composition of organic charge-transfer salts of donor molecules D and acceptor molecules A in the stoichiometry 2 : 1 (top). Certain combinations of building blocks D and A give rise to quasi-1D and quasi-2D electronic structures with pronounced anisotropies of conductivities σ_i along certain crystal axes. Also shown are different arrangements of the donor molecules in the quasi-2D structures (packing motifs) viewed along the long axis of the molecules (bottom). The grey areas represent the unit cells.

differently-shaped acceptor molecules to form a structure shown on the right, where the conductivity along the z-axis will be small compared to the xy-plane conductivity, resulting in a quasi-2D electronic structure. In the lower panel, we show a view from top

along the long axis of the donor molecules (acceptors omitted) revealing different structural arrangements of the molecules, so-called packing motifs. The various packing schemes, labeled by a greek letter, give rise to different molecular overlaps and transfer integrals (see below), and hence correspond to different in-plane electronic properties. Thus, the building block arrangement allows for variations of the dimensionality of the system and subtle modifications of its electronic properties, which in turn lead to the intriguing variety of different ground-state properties observed for these materials.

For theoretical treatment it is convenient and, in many cases, sufficient to consider only either the Highest Occupied Molecular Orbital (HOMO) or the Lowest Unoccupied Molecular Orbital (LUMO) of the π-electrons moving in a potential formed by the σ-electrons together with the nuclei and the inner-shell electrons. This forms the basis of the so-called π-electron approximation. The intermolecular overlaps are calculated from the molecular orbitals. From these overlap integrals, the transfer energy can be directly obtained within the extended Hückel method, see [1] and references therein. The calculated 2D Fermi surfaces are usually rather simple (only slightly corrugated cylinders), and the experimentally determined Fermi surface topologies are in remarkably good agreement with the predictions of the semi-empirical band-structure calculations, see e.g. [7, 8, 9]. Recently, for the materials of interest in this review, these calculations have been refined using first-principle molecular-dynamics methods. These new studies linked the experimental findings with many-body theory by determining the hopping parameters for the underlying Hubbard model [10].

1.2.2 Molecular Building Blocks and Crystal Structures

The organic charge-transfer conductors, on which we focus in this review, are chemically more complicated than most inorganic metals due to the fact that their building blocks are extended, complex molecules rather than point-like atoms. The constituent parts may be viewed as semi-rigid objects owing to the

large difference between the bonding energies within the molecules and the weak intermolecular potentials. This is reflected also in the vibrational frequencies, which consist of *intra*-molecular motional degrees of freedom of the constituent atoms within the molecule and rigid-body motions of the molecular entities themselves, i.e. *inter*-molecular motions or rotations. Correspondingly, the coupling between the conduction electrons and phonons is twofold, involving the *intra*-molecular modes (so-called electron-molecular-vibration coupling) and the electron-*inter*-molecular vibration coupling, which refers to the interaction of the charge carriers with motions of almost rigid molecules around their equilibrium positions and orientations (translational and librational modes). The former coupling relates to the modulation of the HOMO energy by the atomic displacements, and the latter to the modulation of the effective charge-transfer integrals between neighboring molecules during their translational or librational motions. It is an important characteristics of this class of materials, that the relatively soft crystal lattices make their physical properties highly susceptible to changes in external parameters such as temperature or pressure.

Historically, the prototype organic charge-transfer salt is the compound TTF-TCNQ (donor and acceptor molecules shown in Fig. 1), which was synthesized in 1973 [11, 12]. It is a relatively good conductor down to $60\,\mathrm{K}$, where — owing to the inherent instability of one-dimensional electron systems to undergo a MIT — a sharp transition into a nonconducting charge-density-wave ground state occurs. Based on the archetype donor molecule TTF, organic chemistry then provided a vast number of possible molecules that furnish organic conductors. TMTSF, a derivative of the TTF molecule, provides the basis for the so-called Bechgaard salts $(TMTSF)_2X$, which form with a variety of inorganic monovalent octahedral or tetrahedral acceptor molecules X. Figure 4 shows the crystal structure of $(TMTSF)_2PF_6$ (see also Fig. 2), the material, where in 1980 superconductivity had been observed for the first time in an organic compound [13].

The most important members of the second generation of organic conductors are based on the donor
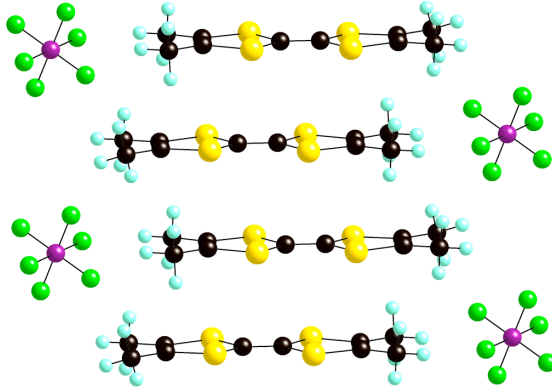

Figure 4: Crystal structure of $(TMTSF)_2PF_6$ viewed from somewhat tilted angle relative to the *b*-direction. The axis of highest conductivity is the stacking *a*-direction, where the molecular orbitals' overlap is largest. Courtesy of J.A. Schlueter, Argonne National Laboratory.

molecule BEDT-TTF (ET), characterized by an enlarged π-electron system. This enhances the overlap between π-orbitals of adjacent molecules when forming the crystal. In contrast to the Bechgaard salts, where the donor molecules form infinite stacks, steric effects specific to the ET molecules prevent such an infinite face-to-face stacking in the $(ET)_2X$ salts. As a consequence, the side-by-side overlap between π-orbitals of adjacent molecules becomes stronger and, in some cases, comparable to the face-to-face interaction resulting in a quasi-2D electronic structure of the ET-based salts. The intermolecular electronic interactions are mostly determined by the hetero-atoms' S contacts, both due to their larger size compared to the C atoms and their location at the periphery of the molecule [14]. The combination of ET with the monovalent anion $X = Cu(NCS)_2$ achieved in 1988 led to the discovery of an ambient-pressure superconductor with a transition temperature in the range of $10\,\mathrm{K}$ [15].

While all members of the $(TMTSF)_2X$ family share the same crystal structure, the rather loose intrastack coupling of the $(ET)_2X$ salts gives rise to a variety of polymorphic phases (packing motifs, see Fig. 3), which are distinguished by Greek characters;

the most important amongst them are the α-, β-, κ-, θ-, and λ-phases. In this review we will focus on the κ-phase materials. This packing is unique in that it does not consist of interacting stacks but rather of interacting dimers formed by two face-to-face aligned ET molecules. Adjacent dimers are arranged almost orthogonal to each other so that the *intra-* and *inter-dimer* interactions are of the same size. This results in a quasi-2D electronic structure with a small in-plane anisotropy. The κ-type compounds with polymeric anions X, as e.g. X = $Cu(NCS)_2$, are of particular interest with respect to their superconducting properties as they exhibit the highest transition temperatures of this class of materials.

The neutral ET molecule $C_6S_8[(CH_2)_2]_2$ [16] is slightly distorted from planar geometry. However, in forming the crystal, the charged ET molecules untwist at their center and become planar, apart from the $[(CH_2)_2]$ (ethylene) groups at the outer ends of the molecules. As shown schematically in Fig. 5, the relative orientation of the outer C−C bonds can either be parallel (eclipsed) or canted (staggered). At high temperatures, these ethylene endgroups are disordered due to strong thermal vibrations. Upon cooling to low temperatures, the endgroups adopt one of the two possible conformations, depending on the anion and the crystal structure, see [1, 3], and Section 1.3.1 below.

κ-(ET)$_2$X Salts with Polymeric Anions X Despite their complex crystal structure with rather low symmetry, it is convenient to think of the $(ET)_2X$ compounds as layered systems consisting of conducting sheets formed by the ET molecules, which are intersected by insulating anion layers, see Fig. 6. Prime examples are the κ-phase $(ET)_2X$ salts with X=$Cu(NCS)_2$, $Cu[N(CN)_2]Br$ and $Cu[N(CN)_2]Cl$, which are the most intensively studied and best characterized members of this class of materials. These compounds are of particular interest, not only because of their relatively high superconducting transition temperatures but also owing to certain similarities in their normal- and superconducting-state properties with those of the high-temperature cuprate superconductors [17, 18]. Figure 6 displays the crys-
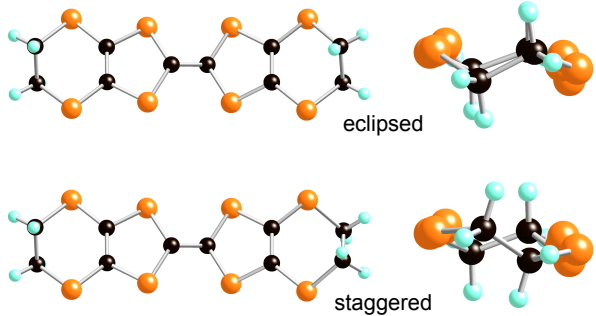

Figure 5: ET molecule $C_6S_8[(CH_2)_2]_2$ [16] and schematic view of the relative orientations of the ethylene endgroups $[(CH_2)_2]$ with eclipsed (top) and staggered conformation (bottom). On the right, the view along the long axis of the molecule is shown. Courtesy of J.A. Schlueter, Argonne National Laboratory.

tal structure of κ-(ET)$_2$Cu[N(CN)$_2$]Z, where Z = Br or Cl. The layered structure consists of conducting planes with the characteristic κ-type arrangement of the ET molecules (see Fig. 3) separated by thin insulating anion layers. While the crystal structure of κ-(ET)$_2$Cu(NCS)$_2$ has monoclinic symmetry with two dimers, i.e. two formula units per unit cell, the κ-(ET)$_2$Cu[N(CN)$_2$]Z salts are orthorhombic with a unit cell containing four dimers. Due to the particular polymeric arrangement, the anions lack a center of inversion symmetry. Subtle changes in the intermolecular spacing or relative orientation of the ET molecules, as e.g. induced by either external pressure or anion substitution, may significantly alter the π-electron overlap between adjacent molecules. This can have a severe influence on the electronic properties as will be discussed in the following.

1.3 Physical Properties of the κ-(ET)$_2$X Salts

In ordinary metals, electrons are usually treated as *nearly-free electrons*. The mutual Coulomb interaction between the charge carriers is effectively screened, so that the quasiparticle mass is only weakly renormalized. Electronic correlation effects,
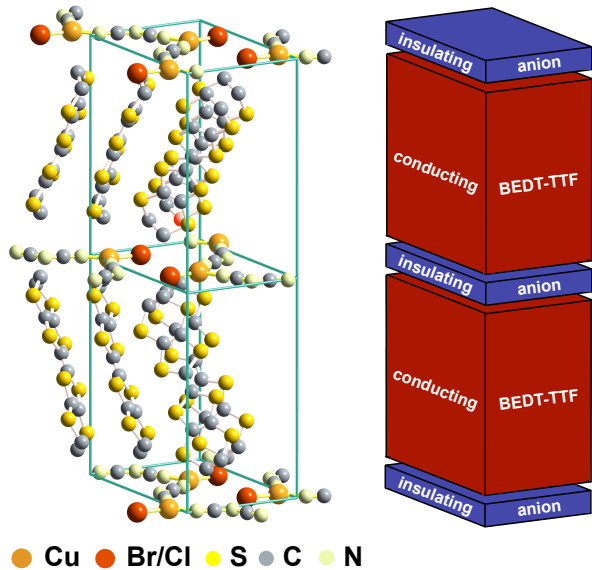
● **Cu** ● **Br/Cl** ● **S** ● **C** ● **N**

Figure 6: Crystal structure of κ-(ET)$_2$Cu[N(CN)$_2$]Z with Z = Br or Cl and schematics showing the layered structure of alternating conducting and insulating blocks. The direction perpendicular to the conducting plane is the crystallographic b-axis. The anion layers are parallel to the ac-plane. The polymeric-like anion chains are running along the a-direction.

however, become important, when the Coulomb interaction between electrons becomes comparable to their kinetic energy, i.e. when $E_{\text{Coul}}/E_{\text{kin}} \sim 1$. Before we discuss the interesting phase diagram of the (ET)$_2$X salts, we briefly outline why these materials are to be characterized as *correlated electron systems*. The stoichiometry of 2 : 1 determines the degree of filling of the conduction band formed by the donor's HOMO to three-quarter-filled by electrons (quarter-filled by holes). Due to the structural dimerization of the ET molecules in the κ-phase arrangement, however, a dimerization gap opens and splits the conduction band into two parts, resulting in an effectively half-filled situation [19]. In terms of a single-particle picture, which neglects electron-electron interactions, metallic behavior is expected for the half-filled conduction band. This is, however, in contrast to the observation since κ-(ET)$_2$Cu[N(CN)$_2$]Cl is an insulator.

Thus, electron-electron interactions must be taken into account in order to understand the diversity of the electronic ground-state properties. One reason is that the bandwidth W is relatively small and indeed estimated to be of the same order as the effective on-site Coulomb repulsion U_{eff}: $W \sim U_{\text{eff}} \sim 0.5\,\text{eV}$. Another reason is that the relatively low charge carrier concentration (of order $10^{21}\,\text{cm}^{-3}$) in combination with the reduced dimensionality ($\sigma_\parallel/\sigma_\perp \sim 10^2 - 10^3$) result in a reduced screening of the charges, which in turn enhances the mutual Coulomb interaction.

Besides the importance of electronic correlations, we point out that optical spectroscopy, inelastic neutron scattering, and thermal conductivity experiments have shown that there is also a rather strong coupling of the π-electrons to the *intra-* and *inter*-molecular vibrations of the crystal lattice, see e.g. [3]. The combined effects of electron-electron and electron-phonon interactions are experimentally observed in measurements of quantum oscillations (Shubnikov-de Haas and de Haas-van Alphen experiments) and the heat capacity, aiming to determine the effective masses of the charge carriers m^*. It is found that $m^* = (1 + \lambda_{\text{el}-\text{el}} + \lambda_{\text{el}-\text{pho}})\,m_e = (3.5 - 7)\,m_e$, where m_e is the free electron mass. It is fair to say, that both the Coulomb interaction between electrons and their coupling to the lattice degrees of freedom (represented by the coupling parameters $\lambda_{\text{el}-\text{el}}$ and $\lambda_{\text{el}-\text{pho}}$, respectively) contribute to the enhanced effective quasiparticle masses. Thus, the materials can be viewed as model systems for low-dimensional metals with both strong electron-electron and electron-phonon interactions.

Figure 7 is a schematic representation of the phase diagram of the κ-phase (ET)$_2$X salts with polymeric anions X (after [20, 21, 22, 23, 24, 25]). Shown is the temperature of the various phase boundaries and other transition/crossover lines as a function of hydrostatic pressure or chemical composition. The arrows indicate the ambient-pressure position of systems with different anions X. For example, κ-(ET)$_2$Cu[N(CN)$_2$]Cl is an antiferromagnetic insulator at ambient pressure with a Néel temperature of $T_N = 27\,\text{K}$. Application of a small hydrostatic pressure of only 300 bar drives the system into a superconducting ground state with $T_c = 12.8\,\text{K}$, [26, 27, 28].
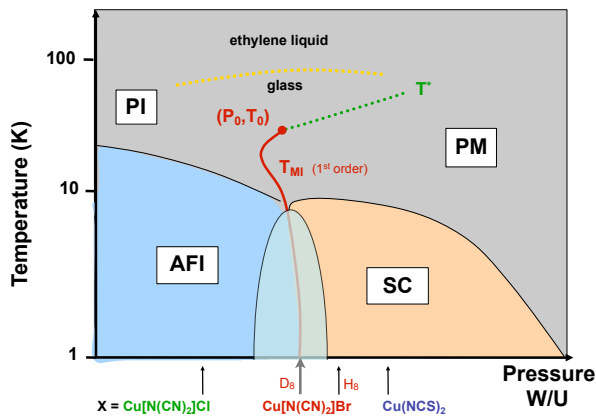
Figure 7: Schematic temperature-pressure (T-P) phase diagram of κ-(ET)$_2$X, after [20, 21, 22, 23, 24, 25]. Arrows indicate the positions of compounds with different anions X at ambient conditions. PI, PM, AFI and SC denote paramagnetic insulating, paramagnetic metallic, antiferromagnetic insulating and superconducting ground states, respectively. It was first proposed by K. Kanoda [21] that these electronic phases are controlled by a single parameter U_{eff}/W.

The same effect is observed, when replacing Cl in the anion complex by Br: κ-(ET)$_2$Cu[N(CN)$_2$]Br is an ambient-pressure superconductor with $T_c = 11.6\,\mathrm{K}$ [29], demonstrating the universality of the phase diagram.

1.3.1 Important Aspects of the Phase Diagram

It is now commonly agreed, that the P, X (pressure and chemical substitution, respectively) axis of the phase diagram (Fig. 7) can be mapped onto the strength of the effective on-site (dimer) Coulomb repulsion U_{eff} relative to the width of the conduction band W. The underlying idea is that hydrostatic pressure or certain changes in the anion structure increase the overlap of the molecular orbitals of adjacent molecules leading to a more metallic behavior. Accordingly, Fig. 7 shows a concept of a phase diagram for the strongly dimerized (ET)$_2$X salts [21, 30], which is based on the strongly cor-

related nature of the π-electrons and assumes that the ground state is controlled by a single parameter U_{eff}/W [31, 21]. This idea, first proposed by K. Kanoda [21, 30], offers intriguing possibilities for applying and testing the fundamental theoretical models of strongly-correlated electron physics, as e.g. the extended Hubbard model, see [3] and references therein. According to this phase diagram, the antiferromagnetic insulator X = Cu[N(CN)$_2$]Cl and the correlated metal κ-(ET)$_2$Cu[N(CN)$_2$]Br lie on opposite sides of a bandwidth-controlled Mott transition. The Mott transition is a type of MIT of particular recent interest, where a gap opens in the charge-carrying excitations due to electron-electron interactions. As already mentioned, Mott insulators have an odd number of conduction electrons per unit cell and, according to band theory, should be metals. However, if the ratio of the on-site correlation energy U to the kinetic energy W becomes larger than a critical value, all electrons localize. The S-shaped Mott MIT line (red line in Figs. 7) is of first order and terminates in a critical endpoint (P_0, T_0). The deuterated variant κ-(D$_8$-ET)$_2$Cu[N(CN)$_2$]Br, where the Hydrogen atoms of the ethylene endgroups of the ET molecules are substituted by Deuterium is situated right at the antiferromagnetic insulator (AFI) to superconductor (SC) phase boundary [32]. The close proximity of an antiferromagnetic insulating to a superconducting phase has been considered — in analogy to the high-T_c cuprates — as an indication that both phenomena are closely connected to each other, see e.g. [18].

We conclude this section with a brief overview of some important and currently intensively investigated aspects of the phase diagram, beginning with the properties of the normalconducting state at elevated temperatures.

The Glass-Like Transition Often, in materials based on complex organic molecules, the internal degrees of freedom of the constituent structure elements give rise to a glass-like behavior. This is related to relaxation processes, where — for kinetic reasons — below a characteristic temperature denoted as the glass-transition temperature T_g, the motion of certain molecular units become so slow that thermo-

dynamic equilibrium cannot be achieved anymore. Materials like this, which are characterized by disorder with respect to the orientational degrees of freedom of the translationally ordered molecules are called 'plastic crytals' [33]. These are often considered as model systems for 'conventional' glass formers as their properties resemble that of glass-forming liquids in many respects. For κ-(ET)$_2$Cu[N(CN)$_2$]Cl and κ-(ET)$_2$Cu[N(CN)$_2$]Br, at $T_g \sim 70 - 80$ K (dotted yellow line in Fig. 7), a glass-like transition has been identified in measurements of thermodynamic quantities as the heat capacity [34, 35, 36] and the coefficients of thermal expansion [23, 37, 38]. The conformational degrees of freedom of the ET molecules' ethylene endgroups described in Section 1.2.2 above are the obvious candidates for such a glassy behavior (see Fig. 5). The transition marks the boundary between an ethylene-liquid at $T > T_g$ and a glassy state at $T < T_g$. At temperatures above T_g, a certain fraction of the ethylene endgroups is thermally excited, i.e. there are switching processes between two possible conformations, with a preferential occupancy of one of these orientations depending on the anion, in case of κ-(ET)$_2$Cu[N(CN)$_2$]Z in the eclipsed configuration. Upon cooling through T_g, however, these orientational degrees of freedom freeze-in within a narrow temperature interval. Thus, the cool-down of the sample is accompanied by a certain amount of disorder in the ethylene endgroups becoming frozen below T_g. The degree of this *intrinsic* type of disorder can be controlled by varying the cooling rate at T_g. Accordingly, the glass-like transition, which is structural in nature, has been shown to cause time dependencies of the electronic properties and may have severe implications on the ground-state properties of the κ-(ET)$_2$Cu[N(CN)$_2$]Br salt depending on the degree of frozen disorder, see discussion in [3].

The Unusual Normalconducting State Besides these glassy anomalies at higher temperatures, pronounced anomalies in the coefficient of thermal expansion have been found at intermediate temperatures T^* reminiscent of a broadened second-order phase transition [23, 39]. These anomalies coincide with features in various thermal [40, 41, 42, 43], magnetic [44, 45, 46, 47, 48], acoustic [49, 24] and optical properties [50]. Various explanations have been proposed as to the nature of the anomaly at T^*, including the formation of a pseudo-gap in the density of states [44, 45, 46, 47], a crossover from a coherent Fermi liquid at low temperatures into a regime with incoherent excitations ("bad metal") at high temperatures [51, 52], a density-wave-type instability [23, 43, 39], as well as an incipient divergence of the electronic compressibility caused by the proximity to the Mott transition [24]. Recent thermodynamic studies [53, 54] suggest that the broadened mean-field like features at T^* observed on the metallic side far from the critical point develop into a critical behavior when approaching (P_0, T_0). This means that either T^* marks a line of phase transitions merging into the critical point (P_0, T_0) of the Mott transition (making the latter a tricritical point rather than a critical endpoint), or the $T^*(P, X)$ line is a crossover line, an extension of $T_{MI}(P, X)$, and the observed effects may be explained in the framework of scaling behavior near the finite-temperature critical endpoint [55].

The Insulator-to-Metal/Superconductor Transition Of particular interest for an understanding of the unusual normalconducting state and the conditions leading to superconductivity in the κ-phase (ET)$_2$X salts, is the nature of the insulator-to-metal/superconductor transition. The latter can be studied either by hydrostatic or chemical pressure experiments. By chemical means, substitutions on the anion site X allows discrete shifts on the pressure scale of the order of a few hundred bars. A *partial* substitution of the 2×4 Hydrogen atoms of the ET molecules' ethylene endgroups by Deuterium in κ-(ET)$_2$Cu[N(CN)$_2$]Br, however, was found to substantially reduce the pressure steps enabling a fine-tuning across the insulator-to-metal/superconductor transition [56, 57, 58, 59]. The transition from the insulating state to the metallic/superconducting state can be studied in a particularly clean fashion by applying He-gas pressure to the κ-(ET)$_2$Cu[N(CN)$_2$]Cl salt. In this way the pressure-temperature phase diagram close to the MIT has been explored in great detail by

many authors [60, 61, 62, 63, 64, 22, 51, 24, 65, 20] employing a variety of experimental techniques such as resistivity, ac-susceptibility, ^{1}H-NMR and ultrasound velocity. By simultaneous measurements of the ^{1}H-NMR and ac-susceptibility, S. Lefebvre et al. have shown that superconducting and antiferromagnetic phases overlap through a first-order boundary that separates two regions of an inhomogeneous phase coexistence [22]. It has been argued that this boundary curve merges with the first-order line of the MIT at intermediate temperatures. The complex physics in this region of the phase diagram has been attributed to strong spatial inhomogeneities [51]. From the separation of ^{13}C-NMR spectra at low temperatures in the fully deuterated compound — located right at the first-order Mott MIT between the metallic and the commensurate antiferromagnetic state —, the existence of inhomogeneous electronic states originating from a phase separation has been suggested [32]. The new technique discussed in this review, noise spectroscopy, can contribute to the understanding of the phase separation in the critical region of the phase diagram.

Extracted from: J. Müller, *Fluctuation Spectroscopy – A new Approach to Study Electronic Correlations in Organic Molecular Materials*, ChemPhysChem **12**, 1222 – 1245 (2011).

References

[1] T. Ishiguro, K. Yamaji, and G. Saito. *Organic Superconductors*. Springer, Berlin Heidelberg, 2nd edition, 1998.

[2] M. Schwoerer and H.Ch. Wolf. *Organische molekulare Festkörper*. Wiley-VCH, Weinheim, 2005.

[3] N. Toyota, M. Lang, and J. Müller. *Low-Dimensional Molecular Metals*. Springer, Berlin Heidelberg, 2007.

[4] A. Lebed. *The Physics of Organic Superconductors and Conductors*. Springer, Berlin Heidelberg, 2008.

[5] M. Dressel and N. Drichko. *Chem. Rev.*, 104:5689, 2004.

[6] D. Jérome C. Bourbonnais. *Physics World*, September:41, 1998.

[7] J. Wosnitza. *Fermi Surfaces of Low-Dimensional Organic Metals and Superconductors*. Springer, Berlin Heidelberg New York, 1996.

[8] J. Singleton. Studies of quasi-two-dimensional organic conductors based on bedt-ttf using high magnetic fields. *Rep. Prog. Phys.*, 63:1111, 2000.

[9] M. V. Kartsovnik. *Chem. Rev.*, 104:5737, 2004.

[10] H.C. Kandpal, I. Opahle, Y.-Z. Zhang, H.O. Jeschke, and R. Valentí. *Phys. Rev. Lett.*, 103:067004, 2009.

[11] J. Ferraris, D. O. Cowan, J. V. Walatka, and J. H. Perlstein. *J. Am. Chem. Soc.*, 95:948, 1973.

[12] L. B. Coleman, M. J. Cohen, D. J. Sandman, F. G. Yamagishi, A. F. Garito, and A. J. Heeger. *Solid State Commun.*, 12:1125, 1973.

[13] D. Jérome, A. Mazaud, M. Ribault, and K. Bechgaard. *J. Physique Lett.*, 41:L95, 1980.

[14] J. M. Williams, J. R. Ferraro, R. J. Thorn, K. D. Carlson, U. Geiser, H. H. Wang, A. M. Kini, and M.-H. Whangbo. *Organic Superconductors (Including Fullerenes)*. Prentice Hall, Englewood Cliffs, N.J., 1992.

[15] K. Oshima, T. Mori, H. Inokuchi, H. Urayama, H. Yamochi, and G. Saito. *Phys. Rev. B*, 38:938, 1988.

[16] H. Kobayashi, A. Kobayashi, Y. Sasaki, G. Saito, and H. Inokuchi. *Bull. Chem. Soc. Japan*, 59:301, 1986.

[17] M. Lang. *Superconductivity Review*, 2:1, 1996.

[18] R. H. McKenzie. *Science*, 278:820, 1997.

[19] H. Seo, C. Hotta, and H. Fukuyama. *Chem. Rev.*, 104:5005, 2004.

[20] F. Kagawa, K. Miyagawa, and K. Kanoda. *Nature*, 436:534, 2005.

[21] K. Kanoda. *Physica C*, 282 - 287:299, 1997.

[22] S. Lefebvre, P. Wzietek, S. Brown, C. Bourbonnais, D. Jérome, C. Mézière, M. Fourmigué, and P. Batail. *Phys. Rev. Lett.*, 85:5420, 2000.

[23] J. Müller, M. Lang, F. Steglich, J. A. Schlueter, A. M. Kini, and T. Sasaki. *Phys. Rev. B*, 65:144521, 2002.

[24] D. Fournier, M. Poirier, M. Castonguay, and K.D. Truong. *Phys. Rev. Lett.*, 90:127002–1, 2003.

[25] M. Dumm, D. Faltermeier, N. Drichko, M. Dressel, C. Mézière, and P. Batail. *Phys. Rev. B*, 79:195106, 2009.

[26] J. M. Williams, A. M. Kini, H. H. Wang, K. D. Carlson, U. Geiser, L. K. Montgomery, G. J. Pyrka, D. M. Watkins, J. M. Kommers, S. J. Boryschuk, A. V. Strieby Crouch, W. K. Kwok, J. E. Schirber, D. L. Overmyer, D. Jung, and M.-H. Whangbo. *Inorg. Chem.*, 29:3272, 1990.

[27] H. H. Wang, K. D. Carlson, U. Geiser, A. M. Kini, A. J. Schultz, J. M. Williams, L. K. Montgomery, W. K. Kwok, U. Welp, K. G. Vandervoort, S. J. Boryshuk, A. V. Strieby Crouch, J. M. Kommers, D. M. Watkins, J. E. Schirber, D. L. Overmyer, D. Jung, J. J. Novoa, and M.-H. Whangbo. *Synth. Met.*, 41-43:1983, 1991.

[28] Yu. V. Sushko and K. Andres. *Phys. Rev. B*, 47:330, 1993.

[29] A. M. Kini, U. Geiser, H. H. Wang, K. D. Carlson, J. M. Williams, W. K. Kwok, K. D. Vandervoort, J. E. Thompson, D. L. Supka, D. Jung, and M.-H. Whangbo. *Inorg. Chem.*, 29:2555, 1990.

[30] K. Miyagawa, K. Kanoda, and A. Kawamoto. *Chem. Rev.*, 104:5635, 2004.

[31] K. Kanoda. *Hyperfine Int.*, 104:235, 1997.

[32] K. Miyagawa, A. Kawamoto, and K. Kanoda. *Phys. Rev. Lett.*, 89:017003, 2002.

[33] P. Lunkenheimer, U. Schneider, R. Brand, and A. Loidl. *Contemp. Phys.*, 41:15, 2000.

[34] K. Saito, H. Akutsu, and M. Sorai. *Solid State Commun.*, 111:471, 1999.

[35] H. Akutsu, K. Saito, and M. Sorai. *Phys. Rev. B*, 61:4346, 2000.

[36] A. Sato, H. Akutsu, K. Saito, and M. Sorai. *Synth. Met.*, 120:1035, 2001.

[37] J. Müller, M. Lang, F. Steglich, and J.A. Schlueter. *J. Phys. IV France*, 114:341, 2004.

[38] J. Müller. *Thermodynamische Untersuchungen an quasi-zweidimensionalen organischen Supraleitern.* Doctor thesis, TU Dresden, Shaker Verlag, Aachen, 2002.

[39] M. Lang, J. Müller, F. Steglich, J. A. Schlueter, A. M. Kini, and T. Sasaki. *Synth. Met.*, 133 - 134:107, 2003.

[40] K. Murata, M. Ishibashi, Y. Honda, N. A. Fortune, M. Tokumoto, N. Kinoshita, and H. Anzai. *Solid State Commun.*, 76:377, 1990.

[41] Yu. V. Sushko, V. A. Bondarenko, R. A. Petrosov, N. D. Kushch, and E. B. Yagubskii. *J. Phys. I France*, 1:1015, 1991.

[42] L. I. Buravov, N. D. Kushch, V. A. Merzhanov, M. V. Osherov, A. G. Khomenko, and E. B. Yagubskii. *J. Phys. I France*, 2:1257, 1992.

[43] T. Sasaki, N. Yoneyama, A. Matsuyama, and N. Kobayashi. *Phys. Rev. B*, 65:060505(R), 2002.

[44] V. Kataev, G. Winkel, D. Khomskii, D. Wohlleben, W. Crump, K.F. Tebbe, and J. Hahn. *Solid State Commun.*, 83:435, 1992.

[45] H. Mayaffre, P. Wzietek, C. Lenoir, D. Jérome, and P. Batail. *Europhys. Lett.*, 28:205, 1994.

[46] A. Kawamoto, K. Miyagawa, Y. Nakazawa, and K. Kanoda. *Phys. Rev. Lett.*, 74:3455, 1995.

[47] S. M. De Soto, C. P. Slichter, A. M. Kini, H. H. Wang, U. Geiser, and J. M. Williams. *Phys. Rev. B*, 52:10364, 1995.

[48] P. Wzietek, H. Mayaffre, D. Jérome, and S. Brazovskii. *J. Phys. I France*, 6:2011, 1996.

[49] K. Frikach, M. Poirier, M. Castonguay, and K.D. Truong. *Phys. Rev. B*, 61:R6491, 2000.

[50] T. Sasaki, I. Ito, N. Yoneyama, N. Kobayashi, N. Hanasaki, H. Tajima, T. Ito, and Y. Isawa. *Phys. Rev. B*, 69:064508, 2004.

[51] P. Limelette, P. Wzietek, S. Florens, A. Gorges, T. A. Costi, C. Pasquier, D. Jérome, C. Mézière, and P. Batail. *Phys. Rev. Lett.*, 91:016401–1, 2003.

[52] J. Merino and R. H. McKenzie. *Phys. Rev. B*, 61:7996, 2000.

[53] M. Lang, M. de Souza, A. Brühl, Ch. Strack, B. Wolf, J. A. Schlueter, J. Müller, and D. Schweitzer. *Physica C*, page in press, 2006.

[54] M. de Souza, A. Brühl, Chr. Strack, B. Wolf, D. Schweitzer, and M. Lang. *Phys. Rev. Lett.*, 99:037003, 2007.

[55] L. Bartosch, M. de Souza, and M. Lang. *Phys. Rev. Lett.*, 104:245701, 2010.

[56] A. Kawamoto, H. Taniguchi, and K. Kanoda. *J. Am. Chem. Soc.*, 120:10984, 1998.

[57] H. Taniguchi and K. Kanoda. *Synth. Met.*, 103:1967, 1999.

[58] H. Taniguchi, A. Kawamoto, and K. Kanoda. *Physica B*, 284-288:519, 2000.

[59] Y. Nakazawa, H. Taniguchi, A. Kawamoto, and K. Kanoda. *Phys. Rev. B*, 61:R16295, 2000.

[60] Yu. V. Sushko, V. A. Bondarenko, R. A. Petrosov, N. D. Kushch, and E. B. Yagubskii. *Physica C*, 185 - 189:2683, 1991.

[61] J. E. Schirber, D. L. Overmyer, K. D. Carlson, J. M. Williams, A. M. Kini, H. H. Wang, H. A. Charlier, B. J. Love, D. M. Watkins, and G. A. Yaconi. *Phys. Rev. B*, 44:4666, 1991.

[62] Yu. V. Sushko, H. Ito, T. Ishiguro, S. Horiuchi, and G. Saito. *Solid State Commun.*, 87:997, 1993.

[63] H. Ito, M. Kubota, Yu. V. Sushko, N. Kojima, G. Saito, and T. Ishiguro. *Synth. Met.*, 70:925, 1995.

[64] H. Ito, T. Ishiguro, M. Kubota, and G. Saito. *J. Phys. Soc. Japan*, 65:2987, 1996.

[65] F. Kagawa, T. Itou, K. Miyagawa, and K. Kanoda. *Phys. Rev. B*, 69:064511, 2004.